

Temperature scaling pattern dependence on representative concentration pathway emission scenarios

A letter

Yasuhiro Ishizaki · Hideo Shiogama · Seita Emori ·
Tokuta Yokohata · Toru Nozawa · Tomoo Ogura ·
Manabu Abe · Masakazu Yoshimori · Kiyoshi Takahashi

Received: 26 August 2011 / Accepted: 24 February 2012 / Published online: 23 March 2012
© The Author(s) 2012. This article is published with open access at Springerlink.com

Abstract To preserve consistency among developed emission scenarios, the scenarios used in climate modeling, and the climate scenarios available for impact research, the pattern scaling technique is useful technique. The basic assumption of pattern scaling is that the spatial response pattern per 1 K increase in the global mean surface air temperature (SAT) (scaling pattern) is the same among emission scenarios, but this assumption requires further validation. We therefore investigated the dependence of the scaling pattern of the annual mean SAT on GHGs emission scenarios of representative concentration pathways (RCP) and the causes of that dependence using the Model for Interdisciplinary research on Climate 5 developed by Japanese research community. In particular, we focused on the relationships of the dependency with effects of aerosols and Atlantic meridional overturning circulation. We found significant dependencies of the scaling pattern on emission scenarios at middle and high latitudes of the Northern Hemisphere, with differences of >15 % over parts of East Asia, North America, and Europe. Impact researchers should take into account those dependencies that seriously affect their research. The mid-latitude dependence is caused by differences in sulfate aerosol emissions per 1 K increase in the global mean SAT, and the high-latitude dependence is mainly caused by nonlinear responses of sea ice and ocean heat transport to global warming. Long-term trends in land-use and land-cover changes did not significantly affect the scaling pattern of annual mean SAT, but they might have an effect at different timescales.

Electronic supplementary material The online version of this article (doi:10.1007/s10584-012-0430-8) contains supplementary material, which is available to authorized users.

Y. Ishizaki (✉) · H. Shiogama · S. Emori · T. Yokohata · T. Nozawa · T. Ogura · M. Abe · K. Takahashi
National Institute for Environmental Studies, Tsukuba-City, Ibaraki, Japan
e-mail: ishizaki.yasuhiro@nies.go.jp

M. Yoshimori
Atmosphere and Ocean Research Institute, The University of Tokyo, Tokyo, Japan

1 Introduction

In impact research for the Fourth Assessment Report of the Intergovernmental Panel on Climate Change, scenarios were developed and applied sequentially in a linear causal chain that extended from socioeconomic factors to impact assessments (Moss et al. 2010). However, this sequential approach is time consuming and leads to inconsistencies among developed emissions scenarios, the scenarios used in climate modeling, and the climate scenarios available for impact research.

A parallel approach is expected to overcome these inconsistencies. The parallel approach begins with the selection of representative concentration pathways (RCPs) from the many possible future scenarios, which are then used to provide inputs to climate models, such as greenhouse gas (GHG) concentrations, aerosol emissions, and land-use/land-cover changes. Then, climate scenarios based on the RCPs are developed in parallel with the development of new socio-economic scenarios. The new climate scenarios will be integrated with the new socio-economic scenarios by using pattern scaling, which is a relatively simple approximation method (Mitchell et al. 1999; Schlesinger et al. 2000; Mitchell 2003; Harris et al. 2006; Hingray et al. 2007; Ruosteenoja et al. 2007). Thus, the pattern scaling has a vital role in parallel approach.

In pattern scaling, the “scaling pattern” of a climate variable is first estimated by linear regression of future changes in the geographical distribution of a climate variable against changes in the global mean surface air temperature (SAT) using simulations performed by a general circulation model (GCM) under a certain emission scenario. Then, the spatial pattern of changes of a certain climate variable per 1 K increase in the global mean SAT is scaled by using simple climate models, such as energy balance models, and a very wide range of emission scenarios. Finally, regional climatic changes under a wide range of emission scenarios are estimated by multiplying the global mean SAT changes by the scaling pattern.

To date, however, only a few studies have been conducted to validate this method (Mitchell et al. 1999; Schlesinger et al. 2000; Mitchell 2003; Shiogama et al. 2010), although pattern scaling has a key role in impact research for AR5. The applicability of pattern scaling requires further investigation by the climate modeling community, and the findings of this research should be communicated rapidly to researchers conducting integrated assessment modeling and those studying impacts, adaptation, and vulnerability (Moss et al. 2007).

A basic assumption of pattern scaling is that the scaling pattern is the same for different emission scenarios (Shiogama et al. 2010). However, if emissions of aerosols, for example, differ among emission scenarios, then the consequent differences in radiative forcing would result in different spatial patterns of SAT and precipitation. In fact, previous research has shown that the scaling pattern for both SAT and precipitation is dependent on differences in sulfate aerosol concentrations among emission scenarios (Mitchell et al. 1999; Schlesinger et al. 2000; Mitchell 2003; Shiogama et al. 2010). This dependence on emission scenarios can lead to notable differences in impact research (Shiogama et al. 2010).

In general, changes in climate states are caused by changes in radiative forcing, as well as by climate feedback and ocean heat transport processes. The dependence of the scaling pattern on emission scenarios are expected to be strongly related to these climate system mechanisms, but the relationships between these mechanisms and scaling pattern dependencies have not yet been investigated in detail. In particular, the dependencies of the scaling pattern on the RCP scenarios being used for AR5 still need to be examined.

We therefore investigated the dependencies of the SAT scaling pattern on GHGs emission scenarios of RCPs as well as the causes of those dependencies using an atmosphere-ocean GCM developed by the Japanese research community called the Model for Interdisciplinary

Research on Climate version 5 (MIROC5; Watanabe et al. 2010). Mainly we focused on the relationships of the dependencies with the changes in radiation induced by aerosols and ocean heat transport processes. In this paper, we investigated the dependencies and the causes between RCP8.5 and RCP2.6 because the emission scenario dependencies are most significant. Then, we confirmed that the findings are consistent between RCP8.5 and the other scenarios of RCPs.

2 Model description

We used MIROC5 atmosphere-ocean GCM. The horizontal resolutions of the atmospheric and ocean models are T85 and approximately 1° , with 40 and 49 vertical layers, respectively. The aerosol transport-radiation model, called SPRINTARS (Takemura et al. 2000, 2002, 2005), incorporated into MIROC5 can treat both direct and indirect effects of the anthropogenic aerosols, carbonaceous matter (black carbon and organic matter), and sulfate. Changes in aerosol emissions are given by the scenarios.

Sulfate and organic carbon aerosol particles scatter solar radiation, reducing the downward shortwave flux at the surface (Ramanathan et al. 2001; Ramanathan and Carmichael 2008). In addition to this so-called direct effect, these aerosols also influence the microphysical properties of clouds by acting as cloud condensation nuclei. The modifications to the microphysical properties enhance the albedo and lifetime of clouds (first and second indirect effects, respectively) and, hence, lead to dimming at the ground surface (Lohmann and Feichter 2005). We calculated the scaling patterns using four emission scenarios and two simulations: RCP2.6 (van Vuuren et al. 2007), RCP4.5 (Wise et al. 2009), RCP6.0 (Hijioka et al. 2008), RCP8.5 (Riahi et al. 2007), 20th century simulations, and a preindustrial control run. The preindustrial control run was used to remove the influence of model drift. In RCP8.5, RCP6.0 and RCP4.5, the radiative forcing pathway leads to radiative forcing of 8.5 W/m^2 , 6.0 W/m^2 and 4.5 W/m^2 in 2100 respectively, whereas in RCP2.6, the peak radiative forcing of 3 W/m^2 is reached before 2100 and then radiative forcing declines. The equivalent CO₂ concentrations corresponding to 2.6 W/m^2 , 4.5 W/m^2 , 6.0 W/m^2 and 8.5 W/m^2 are approximately 475, 630, 800 and 1310 ppm, respectively (van Vuuren et al. 2007; Wise et al. 2009; Hijioka et al. 2008; Riahi et al. 2007). We analyzed the ensemble mean of three ensemble members for each scenario.

3 Estimation of the scaling pattern

We used the method proposed by Mitchell et al. (1999) to estimate the scaling pattern. In this method, the pattern of change for a climate variable $V(x,i)$ simulated by a GCM at position x and time i are approximated by

$$V * (x, i) = \overline{V}(i) * p(x) \quad (1)$$

where $V * (x, i)$ is the approximated pattern obtained by pattern scaling, $\overline{V}(i)$ is the scaling factor, and $p(x)$ is the scaling pattern. In this study, $\overline{V}(i)$ is the global mean SAT change from the first to the ninth decade in the 21st century (2010s to 2090s), taking the average of the period from 1981 to 2000 in the 20th century simulations as the baseline. $p(x)$ describes how a climate variable $V(x,i)$ changes in position x when global mean SAT rises by 1 K, and it is

obtained as a regression coefficient such that the root mean square differences between the simulated pattern $V(x,i)$ and the approximated pattern $V^*(x, i)$ are minimized, as follows:

$$p(x) = \frac{\sum_{i=1}^9 \bar{V}(i)}{\sum_{i=1}^9 \bar{V}(i)^2} \quad (2)$$

4 Analysis of change in energy budget at the top of atmosphere

Because changes in energy budget at the top of atmosphere (TOA) can cause the difference in scaling pattern among emission scenarios, we investigated the changes in the shortwave (SW) and long wave (LW) radiation at the TOA. As for the changes in SW radiation at the TOA, we used the approximate partial radiative perturbation (APRP) method (Taylor et al. 2007; Yokohata et al. 2008). In this method, the changes of SW radiation at the TOA are decomposed into the contributions from clear-sky atmosphere (SW_{CLR}), cloud (SW_{CLD}), and surface (SW_{SFC}) by a simplified TOA model, respectively. The SW_{CLR} contribution to the changes in the shortwave radiation at the TOA mainly reflects changes in the direct effects of aerosols and water vapor, and is divided into reflectivity and absorption terms. The SW_{CLD} contribution reflects changes in clouds, including the indirect effect of aerosols, and the SW_{SFC} contribution reflects changes in sea ice and snow (ice-albedo feedback) and land use. As for the changes in LW radiation at the TOA, we described them in supplementary text S1.

5 Results and discussion

The general features of the annual mean SAT scaling pattern are roughly similar between RCP2.6 and RCP8.5 (Fig. 1a, b). Overall, the values over land are higher than those over the ocean. In addition, maximum values are observed over the Arctic and minimum values over the ocean areas around the Antarctic. These general features are consistent with previous findings (Mitchell et al. 1999). However, the scaling pattern is significantly dependent on the emission scenario (Fig. S1), in particular over middle and high latitudes in the Northern Hemisphere, with differences of more than 15 % over some regions of Europe, East Asia, and North America (Fig. 1c). Whether these differences are serious depends on the impact research objectives.

As changes of SAT are related to the changes in energy budget in general, we investigated the differences of SW (Fig. 2a) and of LW (Fig. S2a) radiation scaling pattern at the TOA between RCP8.5 and RCP2.6. In these figures, positive values indicate that the changes of SW and LW radiation normalized by the global mean SAT change are larger, and negative values indicate that they are smaller for RCP8.5 than for RCP2.6. Overall, the differences of SW radiation scaling pattern are dominant compared to those of LW radiation. The differences of LW_{CLR} and LW_{CLD} scaling pattern between the two RCPs are small in general, and especially small over most parts of the middle and high latitudes of the Northern Hemisphere (Fig. S2b,c). The differences of LW_{SFC} (Fig. S2d) scaling pattern are not so small over Europe, east parts of North America and East Asia. However, since the changes of LW_{SFC} reflect the changes of SAT (text S1), those are not the cause but the result of the changes of SAT.

The magnitudes in the contributions from SW_{CLR} and SW_{CLD} (Fig. 2b, c) are larger in RCP8.5 than in RCP2.6 over most of the Northern Hemisphere mid-latitude region.

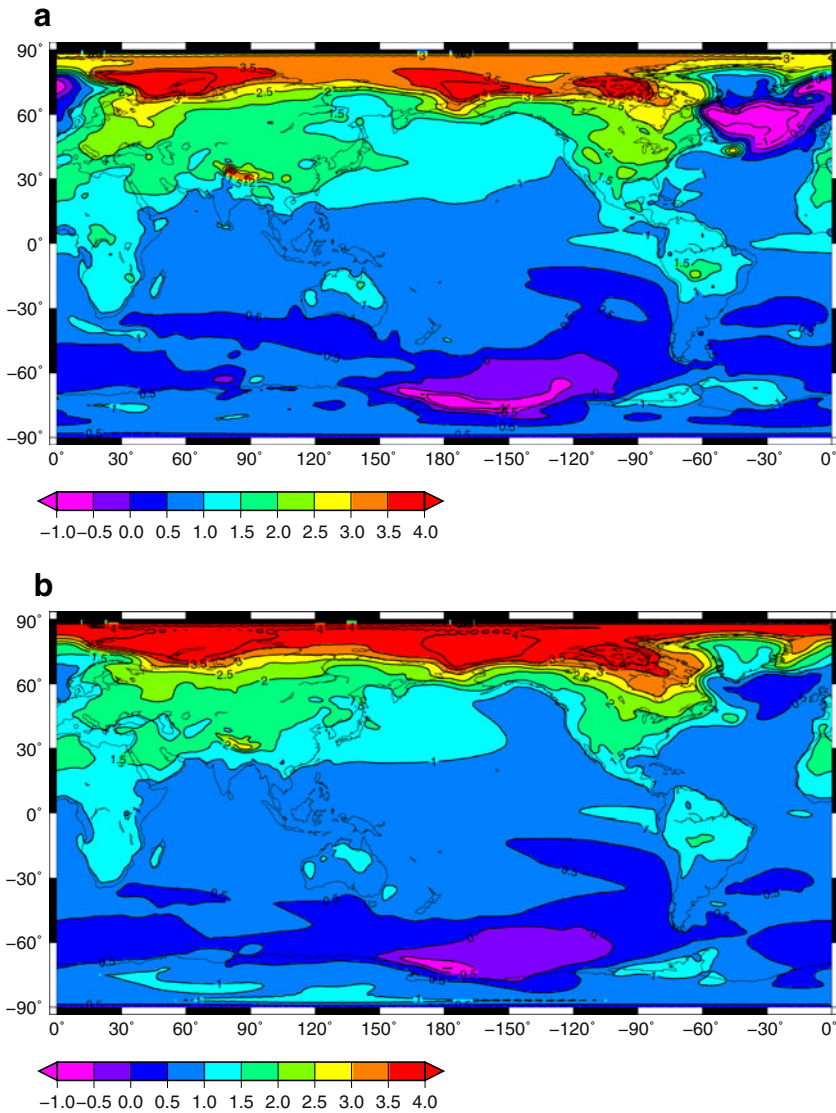


Fig. 1 Scaling patterns (K, per 1 K global mean warming) of annual mean surface air temperature in (a) RCP2.6 and (b) RCP8.5 and (c) its ratios of the differences of scaling patterns of surface air temperature between RCP8.5 and RCP2.6 to that in RCP2.6 (%). Colored regions are statistically significant at the $\alpha=0.05$ level (*F* test)

Spatially, these contributions correspond relatively well to the differences in the scaling pattern of sulfate aerosol between the scenarios (Fig. 3a) over Europe, East Asia, and North America, but not as well to the differences in the scaling pattern of the other aerosols (Fig. 3b, c). However, the scaling pattern values of sulfate aerosol over these regions are smaller in RCP8.5 than in RCP2.6. The difference of global mean of the column loading of sulfate aerosol per 1 K increase in the global mean SAT is large (Fig. S3a). The difference is caused by not only the difference of global mean sulfate aerosol but also that of global mean

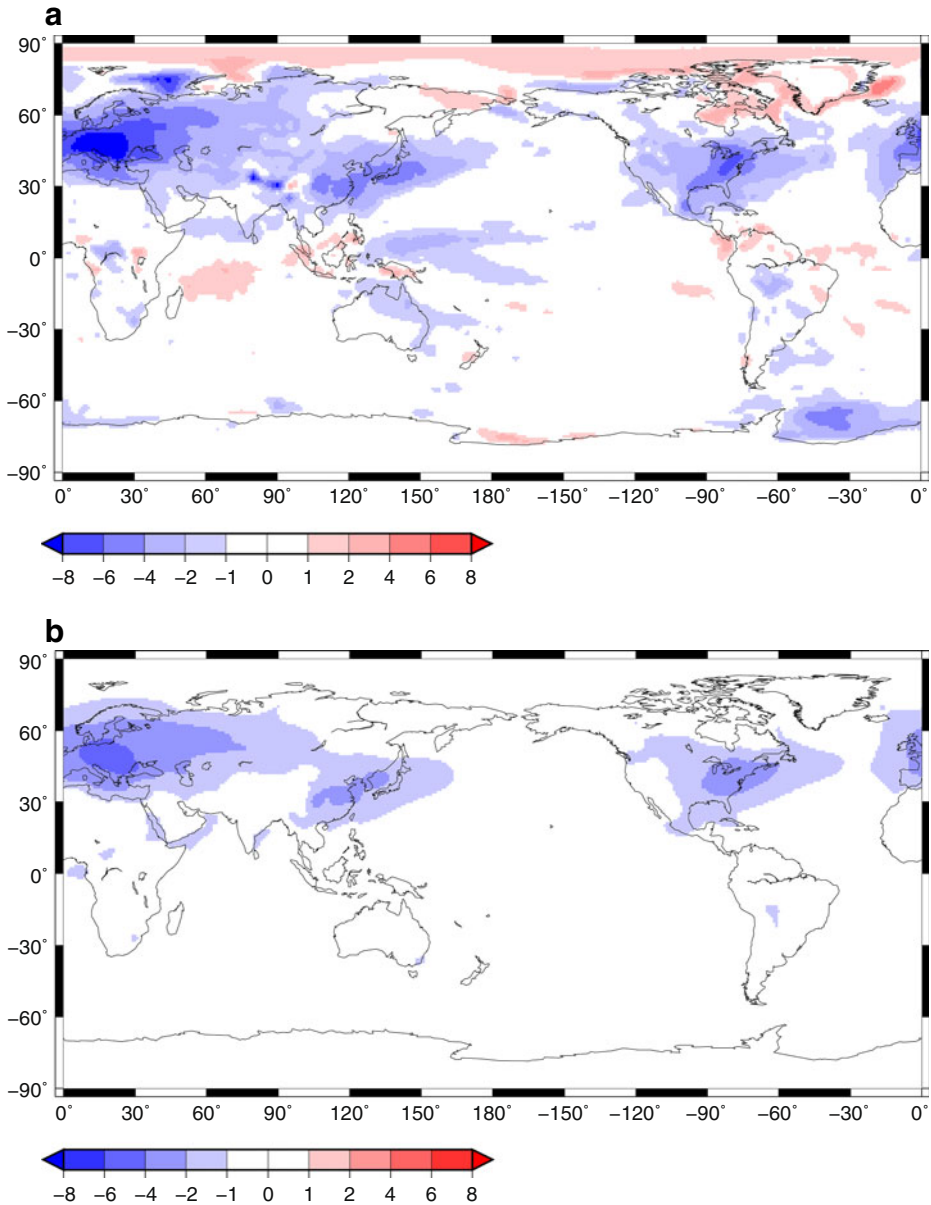


Fig. 2 a Scaling pattern differences in annual mean SW radiation (positive defined downwards) between RCP8.5 and RCP2.6. Contributions to the SW radiation at the TOA: **b** clear-sky atmosphere (SW_{CLR}); **c** cloud (SW_{CLD}); **d** surface (SW_{SFC}). Colored regions are statistically significant at the $\alpha=0.05$ level (F test). All units are W/m^2 , per 1 K change in global mean SAT

SAT change between the two emission scenarios (Fig. S3b,c). The reflectivity term of the SW_{CLR} contribution is dominant over the absorption term (Fig. S4), indicating that the SW_{CLR} contribution to the differences between the scenarios is due mainly to the direct effects of sulfate aerosol. The SW_{CLD} contribution also corresponded well to the scaling

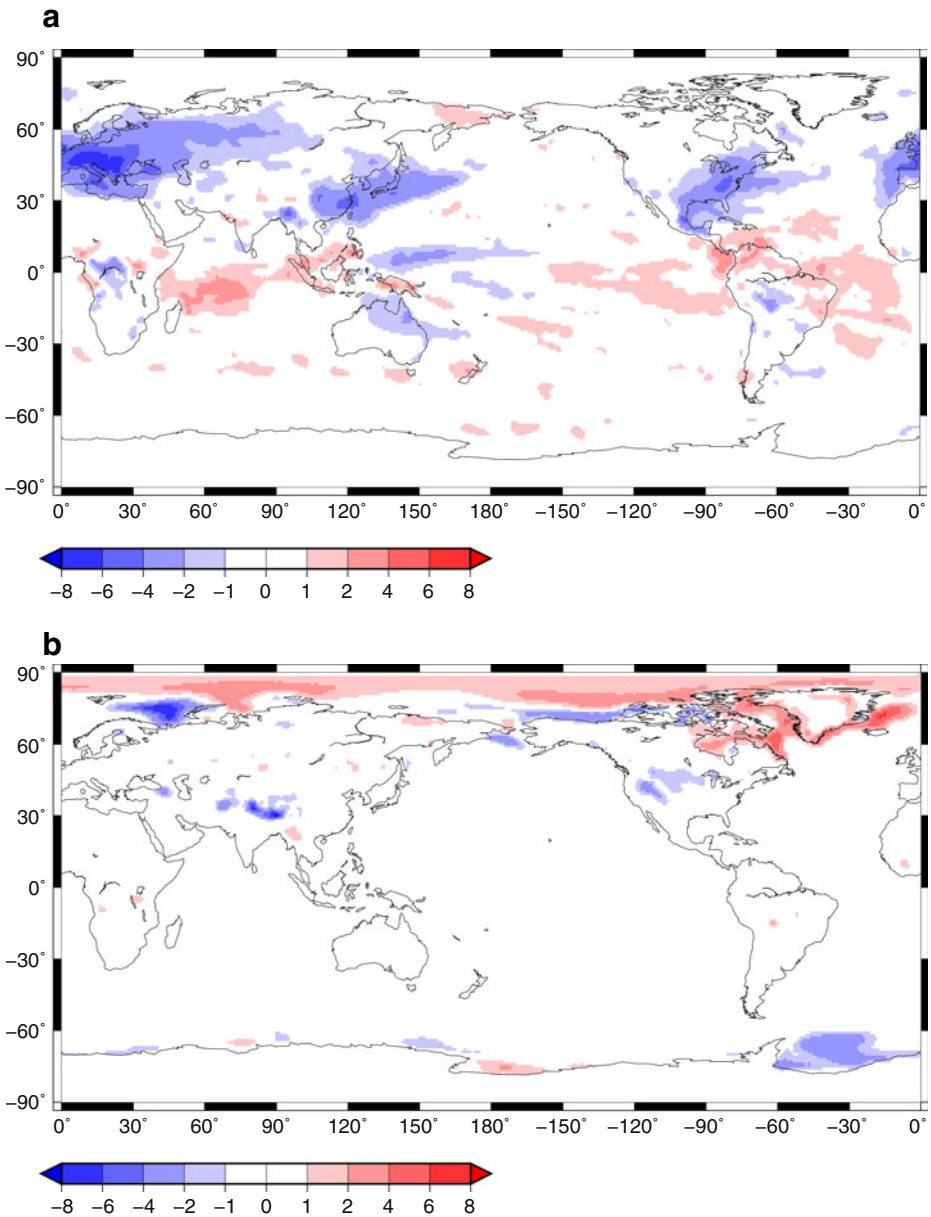


Fig. 2 (continued)

pattern of sulfate aerosol, reflecting the indirect effect of sulfate aerosol. Therefore, the differences in the sulfate aerosol scaling pattern predominantly determine the scenario dependencies of the SAT scaling pattern over Europe, East Asia, and North America through direct and indirect aerosol effects. Although Mitchell et al. (1999) previously reported that direct effects of sulfate aerosol cause dependencies in the SAT scaling pattern, our results

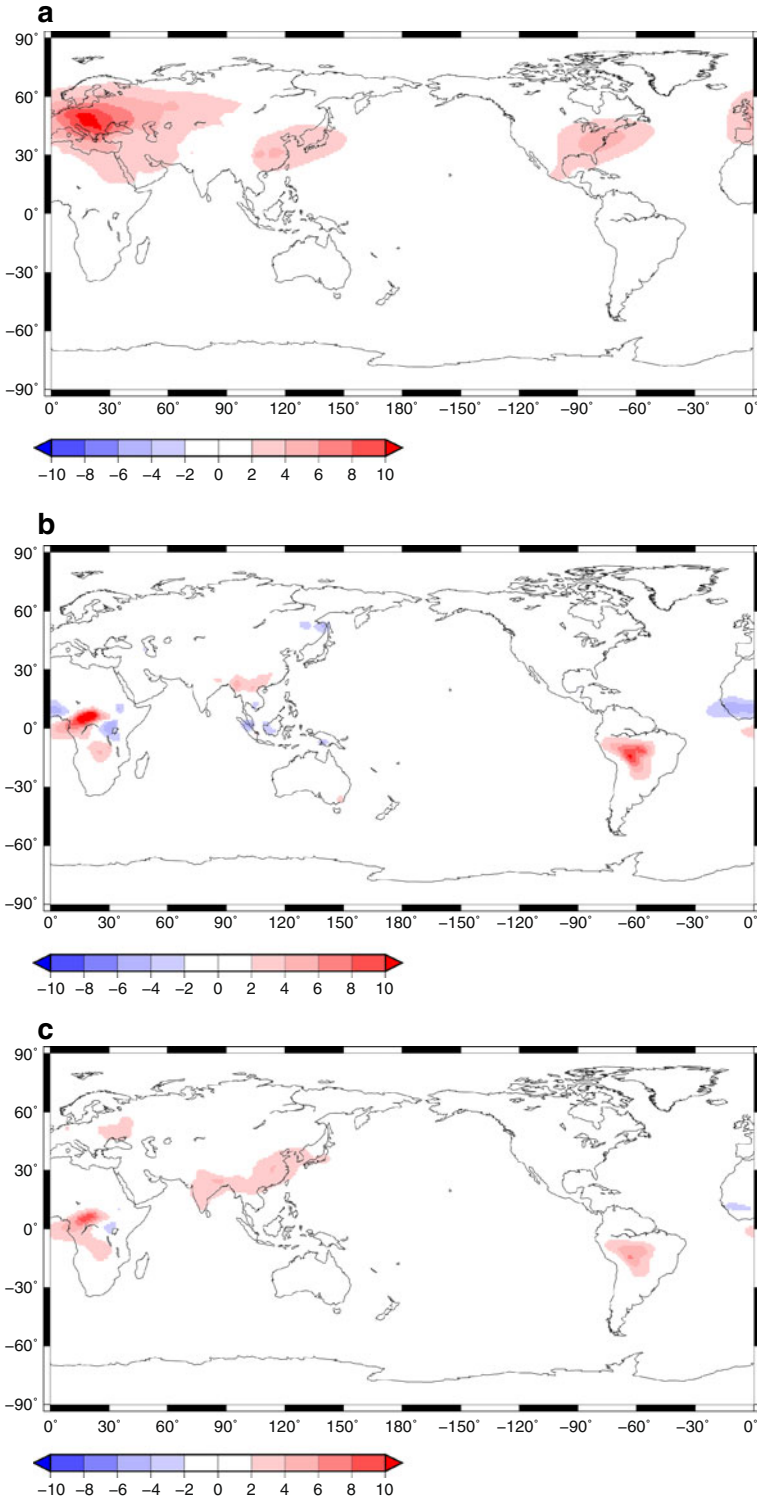


Fig. 3 Scaling pattern differences in annual mean aerosol column loading between RCP8.5 and RCP2.6. **a** Annual mean sulfate aerosol (10^{-6} kg/m², per 1 K change in global mean SAT); **b** annual mean organic carbon (10^{-6} kg/m², per 1 K change in global mean SAT); and **(c)** annual mean black carbon (10^{-7} kg/m², per 1 K change in global mean SAT). Colored regions are statistically significant at the $\alpha=0.05$ level (F test)

show that not only direct effects but also indirect effects are responsible for the dependencies.

Over the Arctic, the scenario dependence of the SAT scaling pattern (Fig. 1) corresponds well to the differences between scenarios in the scaling pattern of the SW_{SFC} contribution at the TOA (Fig. 2d), which corresponds to ice-albedo feedback. The rate of decrease in the sea ice area over the Arctic per 1 K of global warming is increasing as global warming progresses (Fig. 4a), probably because the sea ice is getting thinner under global warming, the ratio of decrease in the sea ice area is smaller in RCP2.6. Thus, the SW_{SFC} contribution over the Arctic at the TOA is increasing nonlinearly as well (Fig. S5). These nonlinear relationships result in different SAT scaling patterns between the scenarios over the Arctic (Fig. 1c).

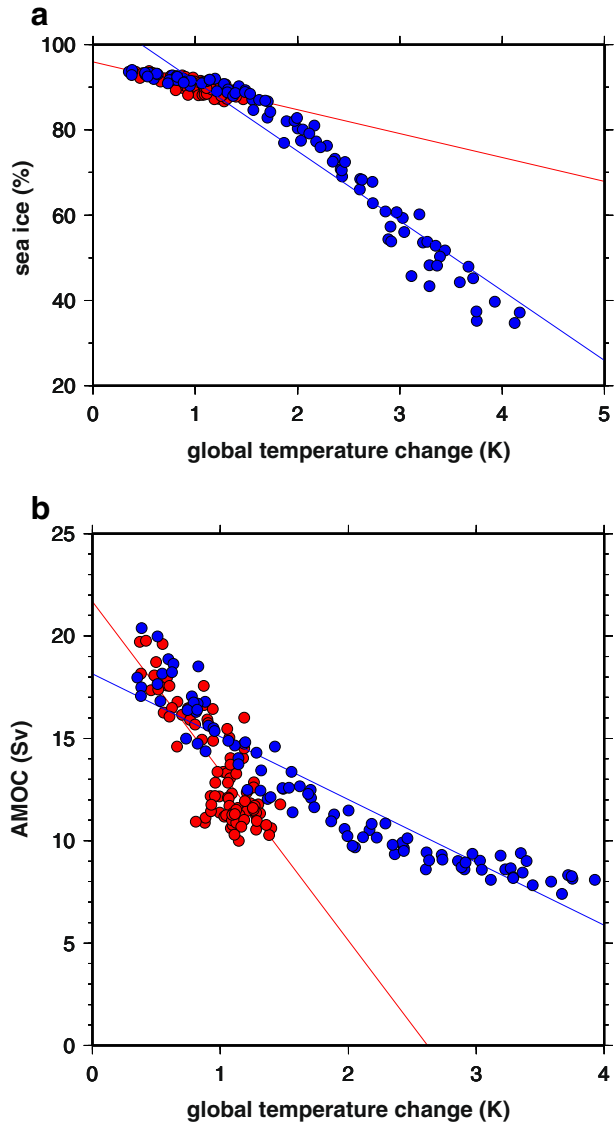
In addition to the nonlinear decrease in sea ice, other factors, such as the temperature lapse-rate feedback, can induce polar amplification (Boe et al. 2009; Yoshimori et al. 2009). In fact, the change in the temperature lapse rate over the Arctic under 1 K of global warming in RCP 8.5 is larger than that in RCP2.6 (data not shown). Thus, the differences in the temperature lapse rate between the two emission scenarios might explain some of the scenario dependence of the SAT scaling pattern over the Arctic.

On the other hand, the SW_{SFC} contribution is not significant over most land areas, even though emission scenarios in the RCP consider long-term trends in land-use patterns (Moss et al. 2010). Thus, long-term trends in land-use patterns are not related to the emission scenario dependence of the annual mean SAT scaling pattern. However, it is possible that at different timescales changes in land-use patterns might influence that dependence.

To the south and east Greenland, SAT is significantly dependent on the emission scenario (Fig. 1c), although no differences in the scaling patterns of SW_{CLR} , SW_{CLD} , or SW_{SFC} (Fig. 2b–d) are evident there between the two emission scenarios. In general, the projected reduction in the Atlantic meridional overturning circulation (AMOC) as a result of increasing GHG concentrations is expected to suppress warming in the North Atlantic region by reducing poleward heat transport (Meehl et al. 2007). In MIROC5, the AMOC response to the global mean SAT change is nonlinear (Fig. 4b) and the decreasing ratio of AMOC strength per 1 K increase in the global mean SAT under global warming in RCP8.5 is smaller than that in RCP2.6. Therefore, differences in heat transport from low to high latitudes per 1 K change in global mean SAT causes the scenario dependence of the SAT scaling pattern to the south and east Greenland. Moreover, the differences in heat transport from low to high latitudes might also influence the scenario dependence of the SAT scaling pattern over the Arctic. The cause of the nonlinear response of the AMOC to increasing GHG concentrations requires further investigation.

The characteristics of CO₂ emissions in RCP2.6 are very different from those of the emission scenarios in the other RCPs, because RCP2.6 aims to limit the increase of global mean temperature to 2°C (van Vuuren et al. 2007). Actually, it achieves an almost equilibrium (Fig. S2S2b). The difference in the CO₂ emission in RCP2.6 may cause a different scenario dependency of SAT scaling pattern. However, the differences of SAT scaling pattern over parts of East Asia, North America, and Europe can be explained by the differences of sulfate aerosol scaling pattern between RCP8.5 and the emission scenarios in the other RCPs (Fig. S6S6a–d). The importance of nonlinear responses of sea ice melting and the decreasing ratio of AMOC to global warming are consistent between them (figure not shown).

Fig. 4 Relationships between (a) ratio of sea ice area over the Arctic and (b) the strength of the Atlantic meridional overturning (AMOC) and global mean surface air temperature changes in annual mean. The ratio of sea ice area over the Arctic is the regional mean from 80°N to 90°N. The intensity of the AMOC is defined as the maximum value of its stream function in the North Atlantic Ocean. Red circles ●, RCP2.6; Blue circles ●, RCP8.5. Red and blue lines indicate the regression lines in RCP2.6 and RCP8.5, respectively



6 Summary

Pattern scaling is useful method to provide climate scenarios for a wide range of emission scenarios that preserve consistency among developed emission scenarios, scenarios used in climate modeling, and climate scenarios available for impact research. The basic assumption of pattern scaling is that the scaling pattern is the same among emission scenarios. In this study, we evaluated this basic assumption of pattern scaling and investigated causes of scaling pattern dependence on emission scenarios.

Such dependence is particularly significant over middle and high latitudes of the Northern Hemisphere between RCP8.5 and RCP2.6, with differences of more than 15 % over parts of East Asia, North America and Europe. A similar dependence over the region is shown

between RCP8.5 and the other RCP scenarios. Impact researchers need to consider whether this dependence seriously influences their results.

The dependencies between RCP8.5 and RCP2.6 are induced by both direct and indirect effects of aerosols, caused by differences in sulfate aerosol emissions per 1 K increase in the global mean SAT over mid-latitudes and the nonlinear response of sea ice and ocean heat transport associated with the AMOC over high latitudes although some of the dependencies are caused by the influences of interannual variability. The dependencies over these regions between RCP8.5 and emission scenarios in the other RCPs can be explained by these factors as well. The importance of nonlinear responses of climate feedback and ocean heat transport to global warming for scaling pattern dependency on emission scenarios is a new finding of our study, although Mitchell et al. (1999) previously reported the importance of direct effects of sulfate aerosols.

Over regions where the dependencies on emission scenarios can be explained by analysis of the shortwave radiation budget, it might be possible to develop a method to reduce these differences based on the climate feedback analysis presented in this study. However, there are still several unsolved issues which need further analysis. Although long-term trends in land-use patterns are not associated with the annual mean SAT dependence on emission scenarios, this does not exclude the possibility that dependencies of extreme events (e.g., daily maximum or minimum SAT) is related to land use. Moreover, the scaling pattern is likely to depend not only on the emission scenario but also on the specific GCM used, because there is still large uncertainty in the responses of aerosols, ocean heat transport and other factors to GHG increases among GCMs. Accordingly, the findings in this study may be model dependent. In addition, the dependencies of other important climate variables such as precipitation or extreme events also have important implications for impact research and thus need to be investigated in future studies.

Acknowledgments This work was supported by the Global Environment Research Fund (S-5-3) of the Ministry of the Environment, Japan. Comments by two anonymous reviewers, and editor are highly appreciated.

Open Access This article is distributed under the terms of the Creative Commons Attribution License which permits any use, distribution, and reproduction in any medium, provided the original author(s) and the source are credited.

References

- Boe J, Hall A, Qu X (2009) Current GCMs' unrealistic negative feedback in the Arctic. *J Clim* 22:4682–4695
- Cess RD et al (1990) Intercomparison and interpretation of climate feedback processes in 19 atmospheric general circulation models. *J Geophys Res* 95:16601–16615
- Harris GR, Sexton DMH, Booth BBB, Collins M, Murphy JM, Webb MJ (2006) Frequency distributions of transient regional climate change from perturbed physics ensembles of general circulation model simulations. *Clim Dynam* 27:357–375
- Hingray B, Mezghani A, Buishand TA (2007) Development of probability distributions for regional climate change from uncertain global mean warming and an uncertain scaling relationship. *Hydrol Earth Syst Sci* 11:1097–1114
- Hijioka Y, Matsuoka Y, Nishimoto H, Masui M, Kainuma M (2008) Global GHG emissions scenarios under GHG concentration stabilization targets. *J Global Environ Eng* 13:97–108
- Lohmann U, Feichter J (2005) Global indirect aerosol effects: a review. *Atmos Chem Phys* 5:715–737
- Meehl GA et al (2007) Global climate projections. In: Solomon S et al (eds) *Climate change 2007: the physical science basis*. Cambridge University Press, Cambridge, pp 747–845
- Mitchell TD (2003) Pattern scaling. An examination of the accuracy of the technique for describing future climates. *Clim Change* 60:217–242

- Mitchell JFB, Johns TC, Eagles M, Ingram WJ, Davis RA (1999) Towards the construction of climate change scenarios. *Clim Change* 41:547–581
- Moss et al (2007) Further work on scenarios report from the IPCC expert meeting towards new scenarios for analysis of emissions, climate change, impacts and response strategies. IPCC Expert meeting report, IPCC, Noordwijkerhout, <http://www.ipcc.ch/pdf/supporting-material/expert-meeting-ts-scenarios.pdf>
- Moss RH, Edmonds JA, Hibbard KA, Manning MR, Rose SK, Carter DP, van TR, Emori S, Kainuma M, Kram T, Meehl GA, Mitchell JFB, Nakicenovic N, Riahi K, Smith SJ, Stouffer RJ, Thomson AM, Weyant JP, Wilbanks TJ (2010) The next generation of scenarios for climate change research and assessment. *Nature* 463:747–756
- Ramanathan V, Carmichael G (2008) Global and regional climate changes due to black carbon. *Nat Geosci* 1:221–227
- Ramanathan V, Crutzen PJ, Kiehl JT, Rosenfeld D (2001) Aerosols, climate, and the hydrological cycle. *Science* 294:2119–2124
- Riahi K, Grubler A, Nakicenovic N (2007) Scenarios of long-term socio-economic and environmental development under climate stabilization. *Technol Forecast Soc Change* 74(7):887–935
- Ruosteenoja K, Tuomenvirta H, Jylhä K (2007) GCM-based regional temperature and precipitation change estimates for Europe under four SRES scenarios applying a super-ensemble patternscaling method. *Clim Change* 81:193–208
- Schlesinger ME et al (2000) Geographical Distributions of temperature change for scenarios of greenhouse gas and sulfur dioxide emissions. *Technol Forecast Soc Change* 65:167–193
- Shiogama H, Hanasaki N, Masutomi Y, Nagashima T, Ogura T, Takahashi K, Hijioaka Y, Takemura T, Nozawa T, Emori S (2010) Emission scenario dependencies in climate change assessments of the hydrological cycle. *Clim Change* 99:321–329
- Takemura T, Okamoto H, Maruyama A, Numaguti A, Higurashi A, Nakajima T (2000) Global three-dimensional simulation of aerosol optical thickness distribution of various origins. *J Geophys Res* 105:17853–17873
- Takemura T, Nakajima T, Dubovik O, Holben N, Kinne S (2002) Single-scattering albedo and radiative forcing of various aerosol species with a global three-dimensional model. *J Clim* 15:333–352
- Takemura T, Nozawa T, Emori S, Nakajima TY, Nakajima T (2005) Simulation of climate response to aerosol direct and indirect effects with aerosol transport-radiation model. *J Geophys Res* 110:D02202. doi:10.1029/2004JD005029
- Taylor KE, Crucifix M, Braconnot P, Hewitt CD, Doutriaux C, Broccoli AJ, Mitchell JFB, Webb MJ (2007) Estimating shortwave radiative forcing and response in climate models. *J Clim* 20:2530–2543
- van Vuuren D, den Elzen M, Lucas P, Eickhout B, Strengers B, van Ruijven B, Wonink S, van Houdt R (2007) Stabilizing greenhouse gas concentrations at low levels: an assessment of reduction strategies and costs. *Clim Chang*. doi:10.1007/s/10584-006-9172-9
- Watanabe M, Suzuki T, Oishi R, Komuro Y, Watanabe S, Emori S, Takemura T, Chikira M, Ogura T, Sekiguchi M, Takata K, Yamazaki D, Yokohata T, Nozawa T, Hasumi H, Tatebe H, Kimoto M (2010) Improved climate simulation by MIROC5: mean states, variability and climate sensitivity. *J Clim* 23:6312–6335
- Wise MA, Calvin KV, Thomson AM, Clarke LE, Bond-Lamberty B, Sands RD, Smith SJ, Janetos AC, Edmonds JA (2009) Implications of limiting CO₂ concentrations for land use and energy. *Science* 324:1183–1186
- Yokohata T, Emori S, Nozawa T, Ogura T, Kawamiya M, Tsushima Y, Suzuki T, Yukimoto S, Abe-Ouchi A, Hasumi H, Sumi A, Kimoto M (2008) Comparison of equilibrium and transient responses to CO₂ increase in eight state-of-the-art climate models. *Tellus* 60A:946–961
- Yoshimori M, Yokohata T, Abe-Ouchi A (2009) A comparison of climate feedback strength between CO₂ Doubling and LGM experiments. *J Clim* 22:3374–3395